Recent Progress in Black Phosphorus Based Heterostructures for Device Applications

*Zhibin Yang, and Jianhua Hao**

Z. B. Yang, Prof. J. H. Hao

Department of Applied Physics, The Hong Kong Polytechnic University, Hong Kong, People's Republic of China

E-mail: jh.hao@polyu.edu.hk

Keywords: black phosphorus; heterostructures; devices; electronics; two-dimensional

Abstract

The rise of two-dimensional (2D) layered materials has inspired luxuriant research interests in the development of novel nano-devices. Thanks to van der Waals (vdWs) interlayer forces and free of dangling surface bonds, 2D materials are favorable for constructing vertical heterostructures by combining materials with different features. In recent years, ultrathin black phosphorus (BP) is rediscovered as a new member of 2D family and attracts significant research attention due to its outstanding electronic properties and tunable band gaps, which offers new avenue for the creation of novel 2D heterostructures. Here, we summarize the recent development of the heterostructured architectures based on 2D BP nanosheets and emphasize their device characterizations. The stacks of phosphorene with graphene, semiconductors or insulators are reviewed, along with the methods to characterize the corresponding proof-of-concept devices as well as the potential opportunities for the applications in 2D limit, including transistors, optoelectronic devices and sensors with unprecedented functionalities. Finally, the challenges ahead of BP heterostructures are discussed and some future outlooks are suggested.

1. Introduction

The fast expansion of two-dimensional (2D) materials provides an appealing platform for designing heterostructures with new physical characteristics.[1-4] Differing from conventional bulk heterostructures, 2D heterostructures are connected by van der Waals (vdWs) interlayer forces without surface dangling bonds, enabling the assembling of various ultrathin layered materials without the need of considering lattice mismatch.[1,3] The stacking of different 2D materials on top of each other may result in atomically sharp interface with unprecedented functionalities. The ultrathin thickness allows band structure engineering via electrical modulation in the longitudinal direction. Moreover, the excellent mechanical strength and flexibility of the heterostructures provide new insights for wearable applications. Up to now, a lot of 2D vdWs heterostructures have been prepared by assembling various conventional 2D materials, such as graphene,[5,6] monolayer transition metal dichalcogenides (TMDs),[7,8] and hexagonal boron nitride (h-BN).[9,10] A series of proof-of-concept devices based on 2D heterostructures have also been realized and shown remarkable performance, such as photodiodes,[8,11] tunneling devices[6,10] and memory devices.[12,13]

Among the members of 2D family, phosphorene, namely monolayer of black phosphorus (BP) has attracted enormous interests in recent years due to its preeminent electronic properties.[14,15] In general, BP crystal consists of individual layers held together by weak vdWs interactions, with each layer formed by strong in-plane covalent bonds. (**Figure 1**a). Unlike the planar lattice of graphite, the crystal structure of BP is orthorhombic with each layer exhibiting a repeating puckered honeycomb structure along the armchair direction due to the sp^3 hybridization.[16] This unique structural anisotropy issues in its exceptional in-plane anisotropic optical and electrical natures. Unlike graphene, BP features p-type semiconducting nature with high hole mobility, which is propitious for electronic applications. Due to the quantum confinement effect, the 2D BP possess thickness-dependent direct bandgaps, spanning a wide range from 0.3 eV (infrared) for bulk to 2.0 eV (visible) for

monolayer, which is one of the largest coverage of band gaps among 2D materials (Figure 1b).[17-21] The band tunability enables BP to be optimized for certain applications by selecting the proper thickness. Although the investigation on 2D BP is just started over two years, significant advancements have already been made on the demonstration of BP device applications, such as FETs, batteries, memory devices, sensors and thermoelectric applications.[22-25] Even though phosphorene possesses excellent electronic properties and tunable direct optical band gaps, it suffers from oxidization upon exposure in ambient.[26-28] Because of the surface oxide species, the performance of the phosphorene-based devices would strongly degrade when they are prepared or characterized in air. To overcome the issue, the ultrathin BP nanosheets can be protected by a stable capping layer, such as Al_2O_3 or aryl diazonium (Figure 1c).[26,29] Another strategy to prevent the degradation is to stack another 2D material on top of phosphorene, such as graphene or h-BN, forming a vdWs heterostructure, which can greatly enhance the performance of the BP transistors (Figure 1d).[28,30]

The passivation is only the one of the basic functions of the vdWs heterostructures of BP. So far, a number of BP heterostructures, including the stacking with either other 2D materials or conventional oxides have been developed and shown distinct electronic and optoelectronic properties, which are favorable for the device applications in 2D limit.[31-34] To the best of our knowledge, most of the recent review articles on 2D BP are mainly focus on the synthesis and characterization of isolated phosphorene.[16,35,36] Meanwhile, the general overviews of vdWs heterostructures based on various 2D materials as well as the corresponding applications have also been published.[2,3,37] However, a review of specific BP based heterostructures and their device applications has not been given yet although the number of publications on the combination of phosphorene with various materials is rapidly growing in recent years. As formation of heterostructures and exploration of potential applications become one of the next research hotspots of phosphorene, it is advantageous to systematically review the recent publications in this area. In this review, we comprehensive summarize the recent efforts and

progress in the synthesis and device characterization of stacking of 2D BP nanosheets with other material systems, in the sequence of graphene, semiconductors and insulators. Some strategies in improving the performance of devices based on BP heterostructures and potential research directions in the future will also be discussed.

2. BP-graphene heterostructures

With tight packing of sp^2 bonded carbon atoms in a honeycomb crystal lattice, graphene exhibits unique properties, including ballistic electrical transport, chemical inertness and high mechanical stiffness.[38,39] Especially, as a semi-metal with minimal band gap, graphene presents very high carrier mobility, which makes it a popular component for diverse 2D heterostructures. [3] Graphene has already been used as the contact in many 2D devices rather than the channel.[40-42] This approach is also applicable to BP nanosheets because the BP layer would strongly bind to the metal electrode surface, which would degrade the performance of the devices.[43] In this section, the formation of vdW layer-by-layer heterostructures based on graphene and BP will be introduced. The related electronic devices and energy storage devices will also be highlighted.

2.1. Electronic aspects

To study the properties and physics of the graphene-phosphorene heterostructure, a theoretical model has been constructed by the state-of-the-art *ab initio* simulation.[44] **Figure 3a** illustrates the schematic atomic structure of phosphorene on top of graphene, where lattice structures of both two materials are in the equilibrium state. As properties of phosphorene are easily influenced by any strain,[45] a hypothesis is raised that the graphene layer is stretched while the phosphorene lattice is fixed. The obtained strain within graphene is around 1%, which has no obvious influence on the electronic structure of the heterostructure.

The properties of both phosphorene and graphene are free of influences from the formation of the heterostructure. As shown in Figure 3b, the projected electronic structure of the phosphorene is well preserved due to the weak interaction between graphene and

phosphorene. The result confirms that the good properties of each components of the heterostructure can be well conserved, which is significant for the construction of high quality 2D heterostructures. Further study also confirms that there is no obvious difference of the band structure between the stacking of phosphorene-graphene and the pristine phosphorene. From the perspective of device fabrications, the Schottky barrier height (SBH) is one of the important parameters determining the performance of the device. The calculated SBH for the monolayer phosphorene is 0.64 eV. To form an Ohmic-like contact, an external electrical biases is employed in the vertical direction. As shown in Figure 3c, the band structure of phosphorene relative to graphene could be tuned by the applied electric field. The result indicates that the Schottky barrier of the system behaves like p-type when the external field is smaller than 1.8 V/nm. Along with the increasing of the electrical field, the Schottky barrier is possible to switch from p-type to n-type. For the heterostructure based on bi-layer BP and graphene, the electrical field can even induce an Ohmic contact due to the excess charge carriers in the channel. Similar phenomena has also been observed in other 2D heterostructures.[46]

Experimentally, the contacts and stability of BP FETs can be optimized by constructing a 2D heterostructure, where graphene and h-BN act as the source-drain electrodes and the encapsulation layer, respectively (Figure 3d).[47] The graphene contacts in the heterostructure not only reduce the contact resistances due to their unique tunable work function,[48] but also play a vital role in connecting the protection layer of h-BN and the BP channel. In contrast to the nonlinear output characteristics of BP FETs with metal electrodes, the graphene-contacted devices exhibits perfectly linear behavior of I_d-V_d. In addition, as shown in Figure 3e, the mobility of FET based on the BP heterostructure shows relatively weak temperature dependence because of the scarce of the SBH at the graphene contacts.[47] Moreover, the performance of the encapsulated FET is almost stable under both vacuum and ambient circumstance as shown in Figure 3f. On the other hand, the drain current of the un-

encapsulated device is attenuated significantly in air, which leads to a much lower mobility and switching ratio. Therefore, this heterostructure device can effectively keep the pristine electrical properties of ultrathin BP.

Since there is a lone pair electrons at each atom of BP, it enables the charge transport with the out-of-plane atoms.[49,50] On the basis of this consideration, a vertical FETs (VFETs) has been designed by fabricating the heterostructure of graphene and few-layer BP nanosheet as shown in Figure 3g.[51] Thanks to its high conductivity, graphene is employed as the electrode, which enables the gate modulation in a vertical heterostructure.[52,53] The transport characterization of the VFET shows a large on current density of 1600 A/cm^2 and high off-currents as well, which limits the switching ratios of the devices. It is found that the charge transport properties in the BP VFET are highly influenced by the temperature and the gate voltages, leading to two different explanations for the mechanism of carrier transport. According to the Figure 3h, the large drain-source current at high temperature can be interpreted by the thermionic emission over the Schottky barrier of the heterostructure. In the meantime, the large currents at low temperature is induced by the tunneling effect. On the other hand, the on-off ratios of the VFET nearly decrease along with the increasing of the thickness, which is consistent with the thickness dependent trend of the screening effect (Figure 3i).[51] Thus, the short channel effect is another reason for the poor gate modulation. Overall, the characterization of VFETs based on graphene-BP heterostructure confirms the high out-of-plane conductivity of BP channel, which broaden the potential electronic applications of few-layer BP.

2.2. Energy storage applications

2D BP not only exhibits attractive electronic and optical properties, but also possess a very high theoretical specific capacity (~2595 mAh/g) and large interlayer channel size (3.08 Å), which makes it suitable for the energy storage applications.[54] Previous literatures have

reported that BP can be used as the anode in the lithium batteries.[55,56] Compared with lithium, sodium is more suitable for alkali batteries due to the low cost. However, the weak cycling property limits the application of phosphorene for sodium batteries.[57] Recently, the sandwiched heterostructure of BP and graphene has been employed as the anode of the sodium batteries (**Figure 4**a).[58] In this design, graphene not only acts as an elastic buffer layer, which enables the volumetric expansion during the operation of the battery, but also maintains the heterostructure electrochemically active owing to its high conductivity. At the same time, phosphorene provides the sodium ions a short distance for diffusion. As shown in Figure 4b, the heterostructure is synthesized by solution based methods, resulting in the alternating phosphorene and graphene nanosheets (Figure 4c,d). As no chemical reaction happens between graphene and BP, the structure is connected by weak vdWs forces. The characterization of the electrochemical properties has shown large reversible capacity of the hybrid structure, which is obtained as 2440 mAh/g at current rate of 50 mA/g based on the amount of the phosphorene (Figure 4e).[58] This capacity value is as high as 94% of the theoretical specific capacity of BP (2596 mAh/g). Furthermore, a large capacity retention of 85 % has been obtained at a current rate of 50 mA/g after 100 cycles, indicating good electrochemical stability of the heterostructure of phosphorene and graphene.

Previous reports have demonstrated that the solution exfoliated few-layer BP can be used to fabricate all-solid-state supercapacitors with good flexibility, stability and high capacitance of 13.75 F/cm^3.[59] However, due to the high instability, the irreversible feature of phosphorene is the major limitation when directly applying phosphorene for 2D MSCs applications. Recently, the micro-supercapacitors (MSCs) with high energy density have also been developed by the stacking of phosphorene and graphene nanosheets, namely as PG-MSCs.[60] The phosphorene and graphene were fabricated by liquid exfoliation and electrochemically exfoliation methods,[61] respectively, and then were both filtered by a customized interdigital mask before transferring onto the polyethylene terephthalate (PET) substrates (Figure 4f).[60] The

characterization of the heterostructure shows good flexibility, uniformity and high electrical conductivity. The electrochemical characterization has shown that the obtained capacitances (both areal and volumetric) of the PG-MSCs are much superior to those of either the pure graphene or phosphorene based MSCs (Figure 4g). The flexibility and stability of the PG-MSCs have also been characterized under flatting and bending states each for 1000 cycles.[60] During the initial 1200 cycles, the volumetric capacitance increases step by step, and then maintains at a stable value in in the remaining cycles. After 2000 cycles, the capacitance can even conserve ~89.5% of its maximum value, exhibiting excellent stability and flexibility of the PG-MSCs. Overall, the ultrathin thickness, high flexibility and good electronic properties of the heterostructures of phosphorene and graphene are favorable for 2D high performance energy storage devices.

3. BP-semiconductors van der Waals vertical heterostructures

Owing to the unique crystal structure, BP possesses several advantages for the electronic applications in the 2D category, including the direct tunable band gap, large carrier mobility and the in-plane anisotropic transport features. It is noteworthy that ultrathin BP exhibits p-type semiconducting property, which is attractive for the energy-efficient nano-devices[62] and could also be a promising template to form 2D heterojunctions combined with atomically n-type semiconductors. In this section, the synthesis and device demonstrations of the vdWs vertical heterostructures based on phosphorene and 2D n-type semiconductors will be presented. The p-n and multi-layer heterojunctions as well as Esaki diodes will be described in sequence.

3.1 p-n junctions

The p-n junctions are the basic units for fabricating modern semiconductor devices, such as photodiodes, light-emitting diodes, solar cells, et al.. The first 2D vdWs heterostructure based on phosphorene was achieved by exfoliating few-layer BP nanosheets on top of monolayer MoS_2, which is grown by CVD method (**Figure 5**a).[31] From the results of electrical

characteristics of the heterostructure (Figure 5a), well-defined current rectifying characteristic is observed, indicating the formation of p-n heterojunction between BP and MoS_2. Illuminated by a 633 nm laser with power of 1μW, the optoelectronic characteristics of the BP-MoS_2 p-n junction show the maximum responsivity of 418 mA/W, which is about 100 times larger than that of the few-layer BP based phototransistors. [31,63] Moreover, the photocurrent mapping of the p-n junction shows that the photocurrent is nearly distributed within the scope of the heterojunction, which indicates that the photoelectric effect mainly occurs in the junction region (Figure 45). Besides the visible regime, the heterojunction of BP and MoS_2 also exhibits promising sensitivity in the near-infrared (NIR) band as shown in Figure 5c. The photoresponsivity of 1.55 μm incident laser with 1 nW intensity is as high as 153.4 mA/W, which is much larger than that of photodetectors developed by sole BP nanosheets.[64] The outstanding optoelectronic performance of BP-MoS_2 makes the heterojunction as a potential choice for the photodetection devices, especially in the NIR region.

Differing from BP-MoS_2, the carrier types (p-n, p-p or n-n) of heterojunction of BP-WSe_2 can be tuned by the gate modulation, originating from the ambipolar behavior of both two materials.[65,66] By switching the transport types of BP-WSe_2, current rectifying characteristics and photovoitaic properties of the device can be extensively modified, providing new opportunities to develop novel electronic and optoelectronic applications. Based on such consideration, the BP-WSe_2 heterostructure based logic rectifiers and logic optoelectronic devices have been demonstrated.[65] As shown in Figure 5d, the logic rectifier based on BP-WSe_2 heterojunction can precisely switch between distinct rectifying states by exerting external gate biases, revealing good switching behavior of the device. Moreover, the device exhibits good photovoltaic property with EQE of 23 % when it behaves like a p-n diode. On the other hand, the photovoltaic effect is almost negligible when it behaves like p-p or n-n types of heterojunctions. Based on this feature, the logic optoelectronic devices based on BP-WSe_2 have been developed to convert photon to an electric signal by applying external

biases.[65] The device also exhibits large photoresponsivity of 7×10^8 V/W for incident light of 0.4 nW.

Because of the atomically thin thickness, the band alignment at the interface of 2D heterostructures can be effectively tuned by the adsorption of gas molecules, which enables the system to be developed as chemical sensing devices.[67,68] Previous report has shown that FETs based on multilayer BP can work as a chemical sensor of nitrogen dioxide (NO_2) due to the immediate increase in conductivity of the device upon exposure of NO_2.[69] Recently, a chemical sensor made of the vdWs heterostructure of BP and $MoSe_2$ has shown extremely low detection limit and much higher chemical sensitivity to NO_2 compared with the BP-$MoSe_2$ based sensors constructed on the same chip.[70] The surface potential of the device was characterized by the Kelvin probe force microscopy (KPFM), exhibiting almost identical images for the region before and after exposure to NO_2, which testifies good recovery property of the chemical sensor (Figure 5e). The significant enhancement of the gas sensitivity is mainly ascribed to the modulation of SBH in $MoSe_2$ layer.

Apart from the TMDs, 2D BP could also form p-n junctions with the CVD grown n-type ZnO nanowires (Figure 5f).[33] Such unique 2D-1D heterostructure based device exhibits good static rectifying characteristics with large switching ratio of ~10^4 as well as a kHz dynamic rectifying behavior. In addition, the heterostructure was fabricated into junction field effect transistors (JFETs), where ZnO nanowire and BP nanosheets act as the channel and gate, respectively. The demonstration of the resistive-load inverter based on the JFETs of BP-ZnO shows clearly observable kHz switching dynamics, which owes to the vdWs interactions between few-layer BP nanosheets and ZnO nanowires. This work opens a new path for exploring novel heterostructures based on mixed-dimensional materials.

3.2 Multilayered heterojunctions

Bipolar junction transistors

The bipolar junction transistors (BJT) is a type of transistors which employs both holes and electrons as the transport carriers. Because of its additional internal gain, BJT is commonly applied to amplify the weak current. In a BJT based phototransistor, the photocurrent generated by internal photodiode is subsequently amplified by the inherent transistor, resulting in good performance in all aspects, including bandwidth, magnification and photoresponsivity.[71] The bipolar phototransistors based on 2D materials have been designed by vdWs stacking WSe_2, BP and MoS_2 nanosheets (**Figure 6**a).[72] In the heterostructure, few-layer BP acts as the base terminal owing to its high mobility and broadband photoresponse. WSe_2 plays the role of collector, forming a photodiode with BP, which converts the incident light signal to photocurrent. MoS_2 nanosheets is utilized as emitter, which outputs a large number of electrons for amplifying the signal. The interface of BP-MoS_2 can block the hole transport and control the injection behavior of electrons. Based on this tri-layer heterostructure, a proof-of-concept phototransistor is developed, exhibiting a wide range photoresponse from visible to infrared. The responsivities for the incident light of 1550 nm and 532 nm attain 1.12 and 6.32 A/W, respectively (Figure 6b), which are both much larger than the photodiode based on BP-WSe_2. On the other hand, the relationship between the photocurrent gain and the width of the base region is shown in Figure 6c, revealing that the amplification coefficient decreases along with the accretion of the base width. The experiment results are in consistent with the theoretical model, implying the mechanism of the amplification process, which is the weakening of the influence from contact resistance when the device performance is enhanced.

Floating-gate field-effect transistors

Differing from the conventional FETs with only one gate to control the current switching, a floating-gate field-effect transistor (FGFET) has an extra gate between the channel and the

original gate. The additional gate could retain the charge carriers when the power is off, making the FGFETs applicable for nonvolatile memory applications. In the previous studies, 2D heterostructures of MoS_2/graphene and graphene/h-BN/MoS_2 have been developed into FGFETs.[73,74] However, zero band gap of graphene limits the performance of the device. In order to optimize the nonvolatile ambipolar memories, the heterostructure of BP/h-BN/MoS_2 has been developed for the FGFETs, where the few-layer BP nanosheets act as the transport channels (Figure 6d).[75] The h-BN and MoS_2 play the role of tunneling barrier layer and the floating gate, respectively. The FGFETs exhibit a large memory window of around 70 V, which is tunable by modulating the maximum control gate biases (Figure 6e). Owing to the ambipolar electronic properties of phosphorene, the charge carriers can be accommodated in the MoS_2 trapping layer, enabling the BP/h-BN/MoS_2 heterostructure to be developed for high performance logic circuits and memory devices (Figure 6f). The devices exhibits a large type switching ratio of ~10^2 and a pretty good variation of output characteristics from 0.77 to 0.45 V, which thanks to the outstanding electrical properties of 2D BP.

3.3 Negative differential resistance devices

Negative resistance is an unusual electronic property, which describes that the current would decrease when increasing the applied bias in particular circuits. Based on this property, the negative differential resistance (NDR) devices are designed and show folded *I-V* characteristics, which is promising for the multi-valued logic applications.[76,77] Along with the fast expanding of 2D research, NDR devices have been developed based on the 2D heterostructures with high quality interfaces.[78-80] Among these devices, the Esaki diodes, also called tunnel diode, which exhibit a broken band gap induced by the heavy doping, has been developed by the vdWs stacking of 2D BP/$SnSe_2$ nanosheets.[79] As shown in **Figure 7a**, an ultrathin amorphous layer is observed at the interface between BP and $SnSe_2$, resulting in a well-defined p-i-n junction in the device. The *I-V* characteristics of the device at 80 and 300 K all exhibit the typical N-shaped curve of NDR under the positive drain biases (Figure 7b). The

peak to valley current ratio (PVCR) of the forward-bias output characteristics is 2.8 at 80 K and 1.8 at 300 K, respectively. The performance of the device also shows weak dependence on the temperature, indicating that mechanism of the electron transport is mainly induced by the tunneling effect. In addition, the characterization of photoresponse of the device confirms the broken band gap alignment of the junction (Figure 7c). Taking the observed Esaki diode behavior into account, the formation of type III heterostructure is confirmed.

The main drawback of the Esaki diode based on BP/$SnSe_2$ heterostructure is the low PVCR values when comparing with other 2D heterostructures.[76,78] Recently, the heterostructure of BP/ReS_2 has been fabricated into NDR device, exhibiting higher PVCR values of 4.2 and 6.9 at room temperature and 180 K, respectively.[80] As illustrated in Figure 7d, the result of KPFM measurement shows that there is no overlap region for the band gaps of BP and ReS_2, indicating the formation of the broken-gap band alignment of the heterojunction. To explore the mechanism of the carrier transport, the temperature dependent of the device performance has been characterized. The valley current increases along with the temperature because it is dominated by the diffusion current. On the other hand, the peak current is controlled by the tunneling current, which reduces when the temperature increases. Therefore, the obtained overall PVCR values decrease from 6.8 to 4.02 when the temperature varies from 180 K to 300 K as shown in Figure 7e. Furthermore, a ternary inverter has also been developed based on the BP/ReS_2 NDR device and an inherent BP transistor.[80] The output characteristics of the ternary inverter present that the output signals exhibit three different values when the input voltage increases from 5 to 25 V (Figure 7f). The development of NDR devices based on BP heterostructures builds the basis for the future multi-valued logic devices.

4. BP-insulator heterostructures

The insulating materials integrating with ultrathin BP nanosheets will not only serve as a dielectric layer, but also protect the BP layer from degradation in ambient.[81-83] In this section,

the investigations on the heterostructures of phosphorene and insulators, including the 2D h-BN nanosheets and complex oxides, will be reviewed. The corresponding physics and device applications will be highlighted.

4.1 Quantum oscillations in BP/h-BN

The mobility of BP FETs has been largely improved by inserting an h-BN nanosheet between BP and substrates, which enables the observation of the quantum oscillations.[84,85] **Figure 8**a shows the resistances as a function of magnetic field under different gate biases, exhibiting the notable Shubnikov-de Haas (SdH) oscillations for both holes and electrons. As evidenced from the constant period of the SdH oscillation, the 2D transportation feature of the charge carriers is confirmed. Figure 8b illustrates the dependence of the oscillations on the magnetic fields and temperatures. From the resultant curves, several important information can be calculated, such as carrier lifetime, cyclotron mass and Zeeman splitting. In particular, the obtained cyclotron mass of charge carriers of BP/h-BN are much larger than that of bulk materials.[84]

As BP is very unstable, an encapsulation layer of h-BN will effectively improve the performance of FETs based on phosphorene.[86,87] Therefore, a heterostructure of sandwiched BP with h-BN layers has been designed and possesses clean and uniform interfaces, exhibiting a large field-effect mobility of ~1350 $cm^2V^{-1}s^{-1}$ and switching ratio not lower than 10^5 at room temperature.[85] At 1.7 K, the mobility can even attain up to ~2700 $cm^2V^{-1}s^{-1}$, allowing the observation of quantum oscillations in phosphorene under the magnetic fields of over 6 T. In addition, the anisotropic property of phosphorene will also influence the SdH oscillation of the h-BN/BP/h-BN heterostructure. The device along the X- and Y-directions exhibits distinct conductivity at both room temperature and cryogenic temperature (Figure 8c). The quantum oscillation can be observed along the X-direction, while the oscillation is not obvious under a moderate magnetic field along the Y-direction.

The electronic properties of the above BP heterostructures are mainly limited by the impurities and defects at the interface between BP and h-BN nanosheets. To address the shortcoming, the heterostructure of h-BN/BP/h-BN has been constructed on a graphite back gate as shown in Figure 8d.[88] Due to the function of the bottom h-BN layer, the electrons in the graphite substrate can screen the potential from the impurities at the interface between BP and top h-BN layer.[89,90] The device exhibits ultrahigh Hall mobility up to 6000 $cm^2V^{-1}s^{-1}$, which allows the observation of quantum Hall effect (QHE). As shown in Figure 8e, the well-defined quantized plateaus behavior of Hall resistance R_{xy} can be observed when the R_{xx} is vanished at the same magnetic field, which is the typical appearance of the QHE. The observation of QHE in BP heterostructure helps to obtain the information of Landau levels in BP. Recently, the quality of the heterostructure of h-BN/BP/h-BN has been further optimized by fabricating the structure in vacuum conditions (P = 10^{-3} Torr), which can effectively reduce the impurities from the interfaces by weaken the surface adsorption ability of the materials.[87] At temperature of 2 K, the field-effect mobility can reach up to 45000 $cm^2V^{-1}s^{-1}$, which is much larger than those from the earlier reports. Meanwhile, the SdH oscillation and QHE effect with Landau level filling factors down to v=2 are observed as well. Furthermore, the quantum scattering times are nearly independent of bot the gate biases and temperature as shown in Figure 8f and g. Thus, the spin-selective scattering is observed from the behaviors of charge carriers in h-BN/BP/h-BN heterostructure.

H-BN has been proved to be a one of the promising encapsulation layers to preserve the main properties of the phosphorene. At the same time, h-BN layers can also be employed to counteract the variation of band gap in stacked BP. Besides the applications in quantum physics, the recent publications have demonstrated that the heterostructures of BP and h-BN can also be used in tunneling field-effect transistors (TFETs), THz nanodetectors and batteries, exhibiting enhanced performance or unique properties.[83,91,92]

4.2 Switchable optical devices based on BP-oxides

In addition to h-BN nanosheets, the ultrathin conventional dielectric oxides, such as SiO_2 or Al_2O_3, can be applied to package the sensitive BP nanosheets as well as improving the performance of the corresponding devices.[93-95] Recently, a heterostructure of phosphorene sandwiched between two SiO_2 films has been designed and shown arresting stability in ambient for months (**Figure 9a**).[96] The heterostructure has been characterized by a scattering-type scanning near-field optical microscopy (s-SNOM) equipped with ultrafast near-infrared pump/mid-infrared probe, measureing the switchable interface polaritons in SiO_2/BP/SiO_2 heterostructure. Induced by the THz excitation, the density of photocarriers in BP layer allows the plasmon frequency of BP entering the Reststrahlen band of SiO_2, which makes the polariton modes of BP hybridizing with those of SiO_2. The fringes and corresponding FFT pattern of polariton modes of the heterostructure is presented in Figure 9b and c, respectively. The momentum and frequency of the polariton are consistent well with the theoretical calculation. In addition, as the density of photo carriers is controlled by the frequency of excitation, the phonon-plasma-polariton mode of SiO_2/BP/SiO_2 is switchable. As presented in Figure 9d, the fringes of polarions can be clearly observed within the first 5 ps and the fringe separations are nearly independent to the probe delay time. The excellent switching behavior renders SiO_2/BP/SiO_2 heterostructure the potential candidate for high performance ultrafast nano-photonic devices.

Besides the dielectric oxides, the combination of functional 2D materials with transition-metal oxides, which usually exhibit semiconductive and ferroelectric properties, may also lead to unexpected properties.[97-100] Among the transition metal oxides family, strontium titanate (STO) is one of the most widely studied candidates, which has been proved to be an excellent substrate for growth of functional thin films.[101-103] In contrast to SiO_2, STO substrate could affect the performance of devices owing to the strong interaction at the interface. Recently, the heterostructure based on BP and STO has been designed and show remarkable

optoelectronic properties.[34] Figure 9e illustrates the photoresponse of BP/STO under the illumination of both red and UV light alternately. Upon the excitation light is in on and off states in turn, the generated photocurrent exhibits increasing and decreasing trends, respectively, revealing good photoresponse and wonderful reliability of the device. The obtained photoresponsivity of the BP/STO based photoconductive switch is over 10^5 A/W, which is about 10^5 times larger than that of phototransistors fabricated by few-layer BP.[104] Furthermore, the photocurrent is not declined after the light is off for more than 4 h, exhibiting the persistent photocurrent property (Figure 9f). The excellent performance of the device is related to the generation and recombination of electron-hole pair, which is induced by the defects and optical absorption of STO. To further study the light tunable effect on the persistent feature of photocurrent, the temperature dependence of the photoresponse is measured from as low as 50 K to room temperature (Figure 9g). The fitted curves of time constant versus temperature are consistent with the theoretical calculated charge transfer behavior under illumination, confirming that the optical gating effect is the main reason for the performance of device.

5. Conclusions and outlook

The immerse studies on phosphorene have ignited great interests to investigate the characteristics and potential applications of the material. The free of dangling bonds and vdWs interlayer forces make BP suitable forming heterostructures with other 2D materials or ultrathin oxides. Moreover, the good electronic properties, in-plane anisotropy feature and tunable band gaps in a wide range enable 2D BP to create many fit-for-purpose heterostructures, which can give rise to a wide array of ultrathin electronic and optoelectronic devices. To the best of our knowledge, this is the first review on the BP vdWs heterostructures for the device perspective. In this review, we categorize the recent progress from the types of heterojunctions, which illustrates in the sequence of BP/graphene

(semimetal), BP/semiconductors and BP/insulators. Particularly, the stacking of ultrathin 2D films on top of BP would not only protect the phosphorene from the degradation in ambient, but also exhibit some unprecedented features through the band gap engineering or interlayer interactions. As summarized in Table 1, a variety of applications have been developed by the BP heterostructures, covering the FETs, energy storage, sensors and optoelectronics aspects, which exhibit attractive performance with the potential to complement the modern semiconductor technologies.

So far, the design and device demonstration of BP based heterostructure have just come into the starting stage. Despite the amazing potential and considerable progress, some challenges and opportunities to turn these proof-of-concept devices into practical applications exist as follows:

1. To integrate BP based heterostructures into practical devices, the scalable fabrication of 2D layered BP nanosheets is a crucial challenge due to the extreme instability of phosphorene.[105] So far, the primary method for large area growth of 2D materials is CVD. However, it is suitable to produce phosphorene by CVD because of the highly chemical sensitive surface of BP. Recently, our recent study has shown that an amorphous BP film with wafer-scale can be fabricated at low temperature by pulsed laser deposition (PLD).[62,106] The technique employed in our work is a typical physical growth method,[107,108] which is beneficial for synthesizing BP film. However, the crystalline of the film is poor and the performance is much degraded comparing with the exfoliated BP nanosheets. Therefore, it is necessary to develop a rational and scalable method for the growth of phosphorene and its heterostructures with precisely preserving the properties of each materials.

2. Although extensive efforts have been employed on the investigation of devices based on BP vdWs heterostructures, many fundamental issues of the system are still unclear, which may strongly affect the performance of devices. For instance, although the strain related properties of BP flakes have been studied by Raman spectroscopy most recently,[109] the

influence of strain as well as impurities at the interface on the properties of BP based heterostructures should be further explored. Moreover, the mechanism of transportation of charge carriers at the interface needs to be clarified as well.

3. It has been confirmed that well-defined p-n junctions could be formed between BP and typical 2D n-type semiconductors. Thus, it is reliable to develop more kinds of devices based on the heterojunction, such as solar cells, light-emitting diodes and Zener diodes. So far, the theoretical calculations on the excitonic solar cells based on heterostructures of BP and TMDs have been presented.[110] The solar cell models based on stacking of BP with ZrS_2 or $MoTe_2$ result in large power conversion efficiency as high as 12 %, which still need to be confirmed in the way of experiment.

The diverse heterostructures based on BP starts a new research field and devices fabricated by the system are expected to be the building blocks for novel applications with desired properties. In is foreseen that the further progress in the synthesis and device demonstration of BP based heterostructures would potentially lead to real devices in the future.

Acknowledgements

This work was supported by the grants from Research Grants Council of Hong Kong (GRF No. PolyU 153031/15 P), and Collaborative Research Fund (CRF no. HKU9/CRF/13G).

Received: ((will be filled in by the editorial staff))
Revised: ((will be filled in by the editorial staff))
Published online: ((will be filled in by the editorial staff))

References

[1] K. S. Novoselov, A. Mishchenko, A. Carvalho, A. H. Castro Neto, *Science* **2016**, *353*, aac9439.

[2] A. K. Geim, I. V Grigorieva, *Nature* **2013**, *499*, 419.

[3] Y. Liu, N. O. Weiss, X. Duan, H.-C. Cheng, Y. Huang, X. Duan, *Nat. Rev. Mater.* **2016**, *1*, 16042.

[4] D. Jariwala, T. J. Marks, M. C. Hersam, *Nat. Mater.* **2016**, *16*, 170.

[5] L. Britnell, R. V. Gorbachev, R. Jalil, B. D. Belle, F. Schedin, A. Mishchenko, T. Georgiou, M. I. Katsnelson, L. Eaves, S. V. Morozov, N. M. R. Peres, J. Leist, A. K. Geim, K. S. Novoselov, L. A. Ponomarenko, *Science* **2012**, *335*, 947.

[6] T. Georgiou, R. Jalil, B. D. Belle, L. Britnell, R. V. Gorbachev, S. V. Morozov, Y.-J. Kim, A. Gholinia, S. J. Haigh, O. Makarovsky, L. Eaves, L. A. Ponomarenko, A. K. Geim, K. S. Novoselov, A. Mishchenko, *Nat. Nanotechnol.* **2012**, *8*, 100.

[7] Y. Gong, J. Lin, X. Wang, G. Shi, S. Lei, Z. Lin, X. Zou, G. Ye, R. Vajtai, B. I. Yakobson, H. Terrones, M. Terrones, B. K. Tay, J. Lou, S. T. Pantelides, Z. Liu, W. Zhou, P. M. Ajayan, *Nat. Mater.* **2014**, *13*, 1135.

[8] M. S. Choi, D. Qu, D. Lee, X. Liu, K. Watanabe, T. Taniguchi, W. J. Yoo, *ACS Nano* **2014**, *8*, 9332.

[9] S. Wang, X. Wang, J. H. Warner, *ACS Nano* **2015**, *9*, 5246.

[10] L. Britnell, R. V. Gorbachev, R. Jalil, B. D. Belle, F. Schedin, M. I. Katsnelson, L. Eaves, S. V. Morozov, A. S. Mayorov, N. M. R. Peres, A. H. Castro Neto, J. Leist, A. K. Geim, L. A. Ponomarenko, K. S. Novoselov, *Nano Lett.* **2012**, *12*, 1707.

[11] R. Cheng, D. Li, H. Zhou, C. Wang, A. Yin, S. Jiang, Y. Liu, Y. Chen, Y. Huang, X. Duan, *Nano Lett.* **2014**, *14*, 5590.

[12] K. Roy, M. Padmanabhan, S. Goswami, T. P. Sai, G. Ramalingam, S. Raghavan, A. Ghosh, *Nat. Nanotechnol.* **2013**, *8*, 826.

[13] S. Bertolazzi, D. Krasnozhon, A. Kis, *ACS Nano* **2013**, *7*, 3246.

[14] L. Li, Y. Yu, G. J. Ye, Q. Ge, X. Ou, H. Wu, D. Feng, X. H. Chen, Y. Zhang, *Nat. Nanotechnol.* **2014**, *9*, 372.

[15] H. Liu, A. T. Neal, Z. Zhu, Z. Luo, X. Xu, D. Tománek, P. D. Ye, *ACS Nano* **2014**, *8*, 4033.

[16] V. Eswaraiah, Q. Zeng, Y. Long, Z. Liu, *Small* **2016**, *12*, 3480.

[17] H. Liu, Y. Du, Y. Deng, P. D. Ye, *Chem. Soc. Rev.* **2015**, *44*, 2732.

[18] J. Qiao, X. Kong, Z.-X. Hu, F. Yang, W. Ji, *Nat. Commun.* **2014**, *5*, 4475.

[19] F. Xia, H. Wang, Y. Jia, *Nat. Commun.* **2014**, *5*, 1.

[20] G. Bai, S. Yuan, Y. Zhao, Z. Yang, S. Y. Choi, Y. Chai, S. F. Yu, S. P. Lau, J. Hao, *Adv. Mater.* **2016**, *28*, 7472.

[21] P. Hu, Z. Wen, L. Wang, P. Tan, K. Xiao, *ACS Nano* **2012**, *6*, 5988.

[22] S. Lin, S. Liu, Z. Yang, Y. Li, T. W. Ng, Z. Xu, Q. Bao, J. Hao, C.-S. Lee, C. Surya, F. Yan, S. P. Lau, *Adv. Funct. Mater.* **2016**, *26*, 864.

[23] J. S. Kim, P. J. Jeon, J. Lee, K. Choi, H. S. Lee, Y. Cho, Y. T. Lee, D. K. Hwang, S. Im, *Nano Lett.* **2015**, *15*, 5778.

[24] W. Zhu, S. Park, M. N. Yogeesh, K. M. McNicholas, S. R. Bank, D. Akinwande, *Nano Lett.* **2016**, *16*, 2301.

[25] L. Viti, J. Hu, D. Coquillat, W. Knap, A. Tredicucci, A. Politano, M. S. Vitiello, *Adv. Mater.* **2015**, *27*, 5567.

[26] J. D. Wood, S. A. Wells, D. Jariwala, K.-S. Chen, E. Cho, V. K. Sangwan, X. Liu, L. J. Lauhon, T. J. Marks, M. C. Hersam, *Nano Lett.* **2014**, *14*, 6964.

[27] A. Favron, E. Gaufrès, F. Fossard, A.-L. Phaneuf-L'Heureux, N. Y.-W. Tang, P. L. Lévesque, A. Loiseau, R. Leonelli, S. Francoeur, R. Martel, *Nat. Mater.* **2015**, *14*, 826.

[28] R. A. Doganov, E. C. T. O'Farrell, S. P. Koenig, Y. Yeo, A. Ziletti, A. Carvalho, D. K. Campbell, D. F. Coker, K. Watanabe, T. Taniguchi, A. H. C. Neto, B. Özyilmaz, *Nat.*

Commun. **2015**, *6*, 6647.

[29] C. R. Ryder, J. D. Wood, S. A. Wells, Y. Yang, D. Jariwala, T. J. Marks, G. C. Schatz, M. C. Hersam, *Nat. Chem.* **2016**, *8*, 597.

[30] R. A. Doganov, S. P. Koenig, Y. Yeo, K. Watanabe, T. Taniguchi, B. Özyilmaz, *Appl. Phys. Lett.* **2015**, *106*, 10.

[31] Y. Deng, Z. Luo, N. J. Conrad, H. Liu, Y. Gong, S. Najmaei, P. M. Ajayan, J. Lou, X. Xu, P. D. Ye, *ACS Nano* **2014**, *8*, 8292.

[32] H. Liu, Y. Zou, L. Tao, Z. Ma, D. Liu, P. Zhou, H. Liu, S. Wang, *Small* **2017**, 1700758.

[33] P. J. Jeon, Y. T. Lee, J. Y. Lim, J. S. Kim, D. K. Hwang, S. Im, *Nano Lett.* **2016**, *16*, 1293.

[34] F. Liu, C. Zhu, L. You, S.-J. Liang, S. Zheng, J. Zhou, Q. Fu, Y. He, Q. Zeng, H. J. Fan, L. K. Ang, J. Wang, Z. Liu, *Adv. Mater.* **2016**, *28*, 7768.

[35] M. Batmunkh, M. Bat-Erdene, J. G. Shapter, *Adv. Mater.* **2016**, *28*, 8586.

[36] X. Liu, C. R. Ryder, S. A. Wells, M. C. Hersam, *Small Methods* **2017**, *1*, 1700143.

[37] W. Xia, L. Dai, P. Yu, X. Tong, W. Song, G. Zhang, Z. M. Wang, *Nanoscale* **2017**, *9*, 4324.

[38] C. Lee, X. Wei, J. W. Kysar, J. Hone, *Science* **2008**, *321*, 385.

[39] D. Sun, G. Aivazian, A. M. Jones, J. S. Ross, W. Yao, D. Cobden, X. Xu, *Nat. Nanotechnol.* **2012**, *7*, 114.

[40] L. Yu, Y.-H. Lee, X. Ling, E. J. G. Santos, Y. C. Shin, Y. Lin, M. Dubey, E. Kaxiras, J. Kong, H. Wang, T. Palacios, *Nano Lett.* **2014**, *14*, 3055.

[41] T. Roy, M. Tosun, J. S. Kang, A. B. Sachid, S. B. Desai, M. Hettick, C. C. Hu, A. Javey, *ACS Nano* **2014**, *8*, 6259.

[42] C.-J. Shih, Q. H. Wang, Y. Son, Z. Jin, D. Blankschtein, M. S. Strano, *ACS Nano* **2014**, *8*, 5790.

[43] K. Gong, L. Zhang, W. Ji, H. Guo, *Phys. Rev. B* **2014**, *90*, 125441.

[44] J. E. Padilha, A. Fazzio, A. J. R. Da Silva, *Phys. Rev. Lett.* **2015**, *114*, 1.

[45] A. S. Rodin, A. Carvalho, A. H. Castro Neto, *Phys. Rev. Lett.* **2014**, *112*, 176801.

[46] M. Bokdam, P. A. Khomyakov, G. Brocks, Z. Zhong, P. J. Kelly, *Nano Lett.* **2011**, *11*, 4631.

[47] A. Avsar, I. J. Vera-Marun, J. Y. Tan, K. Watanabe, T. Taniguchi, A. H. Castro Neto, B. Özyilmaz, *ACS Nano* **2015**, *9*, 4138.

[48] Y.-J. Yu, Y. Zhao, S. Ryu, L. E. Brus, K. S. Kim, P. Kim, *Nano Lett.* **2009**, *9*, 3430.

[49] L. Shulenburger, A. D. Baczewski, Z. Zhu, J. Guan, D. Tománek, *Nano Lett.* **2015**, *15*, 8170.

[50] X. Luo, X. Lu, G. K. W. Koon, A. H. Castro Neto, B. Özyilmaz, Q. Xiong, S. Y. Quek, *Nano Lett.* **2015**, *15*, 3931.

[51] J. Kang, D. Jariwala, C. R. Ryder, S. A. Wells, Y. Choi, E. Hwang, J. H. Cho, T. J. Marks, M. C. Hersam, *Nano Lett.* **2016**, *16*, 2580.

[52] M. G. Lemaitre, E. P. Donoghue, M. A. McCarthy, B. Liu, S. Tongay, B. Gila, P. Kumar, R. K. Singh, B. R. Appleton, A. G. Rinzler, *ACS Nano* **2012**, *6*, 9095.

[53] W. J. Yu, Z. Li, H. Zhou, Y. Chen, Y. Wang, Y. Huang, X. Duan, *Nat. Mater.* **2012**, *12*, 246.

[54] D. C. S. Souza, V. Pralong, A. J. Jacobson, L. F. Nazar, *Science* **2002**, *296*, 2012.

[55] J. Sun, G. Zheng, H.-W. Lee, N. Liu, H. Wang, H. Yao, W. Yang, Y. Cui, *Nano Lett.* **2014**, *14*, 4573.

[56] C.-M. Park, H.-J. Sohn, *Adv. Mater.* **2007**, *19*, 2465.

[57] T. Ramireddy, T. Xing, M. M. Rahman, Y. Chen, Q. Dutercq, D. Gunzelmann, A. M. Glushenkov, Y. Chen, K. T. Lee, *J. Mater. Chem. A* **2015**, *3*, 5572.

[58] J. Sun, H.-W. Lee, M. Pasta, H. Yuan, G. Zheng, Y. Sun, Y. Li, Y. Cui, *Nat. Nanotechnol.* **2015**, *10*, 980.

[59] C. Hao, B. Yang, F. Wen, J. Xiang, L. Li, W. Wang, Z. Zeng, B. Xu, Z. Zhao, Z. Liu,

Y. Tian, *Adv. Mater.* **2016**, *28*, 3194.

[60] H. Xiao, Z.-S. Wu, L. Chen, F. Zhou, S. Zheng, W. Ren, H.-M. Cheng, X. Bao, *ACS Nano* **2017**, *11*, 7284.

[61] Y. L. Zhong, T. M. Swager, *J. Am. Chem. Soc.* **2012**, *134*, 17896.

[62] Z. Yang, J. Hao, S. Yuan, S. Lin, H. M. Yau, J. Dai, S. P. Lau, *Adv. Mater.* **2015**, *27*, 3748.

[63] M. Buscema, D. J. Groenendijk, S. I. Blanter, G. A. Steele, H. S. J. van der Zant, A. Castellanos-Gomez, *Nano Lett.* **2014**, *14*, 3347.

[64] L. Ye, H. Li, Z. Chen, J. Xu, *ACS Photonics* **2016**, *3*, 692.

[65] D. Li, B. Wang, M. Chen, J. Zhou, Z. Zhang, *Small* **2017**, *13*, 1603726.

[66] P. Chen, T. T. Zhang, J. zhang, J. Xiang, H. Yu, S. Wu, X. Lu, G. Wang, F. Wen, Z. Liu, R. Yang, D. Shi, G. Zhang, *Nanoscale* **2016**, *8*, 3254.

[67] Y. Liu, X. Dong, P. Chen, X. H. Cao, M. B. Chan-Park, H. Zhang, L. J. Li, W. Huang, P. Chen, P. Chen, S. B. Jovanovich, P. S. Krstic, S. Lindsay, X. S. S. Ling, C. H. Mastrangelo, A. Meller, J. S. Oliver, Y. V. Pershin, J. M. Ramsey, R. Riehn, G. V. Soni, V. Tabard-Cossa, M. Wanunu, M. Wiggin, J. A. Schloss, *Chem. Soc. Rev.* **2012**, *41*, 2283.

[68] B. Liu, L. Chen, G. Liu, A. N. Abbas, M. Fathi, C. Zhou, *ACS Nano* **2014**, *8*, 5304.

[69] A. N. Abbas, B. Liu, L. Chen, Y. Ma, S. Cong, N. Aroonyadet, M. Köpf, T. Nilges, C. Zhou, *ACS Nano* **2015**, *9*, 5618.

[70] Z. Feng, B. Chen, S. Qian, L. Xu, L. Feng, Y. Yu, R. Zhang, J. Chen, Q. Li, Q. Li, C. Sun, H. Zhang, J. Liu, W. Pang, D. Zhang, *2D Mater.* **2016**, *3*, 35021.

[71] Kah-Wee Ang, Ming-Bin Yu, Guo-Qiang Lo, Dim-Lee Kwong, *IEEE Electron Device Lett.* **2008**, *29*, 1124.

[72] H. Li, L. Ye, J. Xu, *ACS Photonics* **2017**, *4*, 823.

[73] M. S. Choi, G.-H. Lee, Y.-J. Yu, D.-Y. Lee, S. H. Lee, P. Kim, J. Hone, W. J. Yoo, *Nat.*

Commun. **2013**, *4*, 1624.

[74] S. Bertolazzi, D. Krasnozhon, A. Kis, *ACS Nano* **2013**, *7*, 3246.

[75] D. Li, X. Wang, Q. Zhang, L. Zou, X. Xu, Z. Zhang, *Adv. Funct. Mater.* **2015**, *25*, 7360.

[76] Y. Wu, D. B. Farmer, W. Zhu, S.-J. Han, C. D. Dimitrakopoulos, A. A. Bol, P. Avouris, Y.-M. Lin, *ACS Nano* **2012**, *6*, 2610.

[77] A. Nourbakhsh, A. Zubair, M. S. Dresselhaus, T. Palacios, *Nano Lett.* **2016**, *16*, 1359.

[78] T. Roy, M. Tosun, X. Cao, H. Fang, D.-H. Lien, P. Zhao, Y.-Z. Chen, Y.-L. Chueh, J. Guo, A. Javey, *ACS Nano* **2015**, *9*, 2071.

[79] R. Yan, S. Fathipour, Y. Han, B. Song, S. Xiao, M. Li, N. Ma, V. Protasenko, D. A. Muller, D. Jena, H. G. Xing, *Nano Lett.* **2015**, *15*, 5791.

[80] J. Shim, S. Oh, D.-H. Kang, S.-H. Jo, M. H. Ali, W.-Y. Choi, K. Heo, J. Jeon, S. Lee, M. Kim, Y. J. Song, J.-H. Park, *Nat. Commun.* **2016**, *7*, 13413.

[81] Y. Cao, A. Mishchenko, G. L. Yu, E. Khestanova, A. P. Rooney, E. Prestat, A. V. Kretinin, P. Blake, M. B. Shalom, C. Woods, J. Chapman, G. Balakrishnan, I. V. Grigorieva, K. S. Novoselov, B. A. Piot, M. Potemski, K. Watanabe, T. Taniguchi, S. J. Haigh, A. K. Geim, R. V. Gorbachev, *Nano Lett.* **2015**, *15*, 4914.

[82] S. Sinha, Y. Takabayashi, H. Shinohara, R. Kitaura, *2D Mater.* **2016**, *3*, 35010.

[83] G. C. Constantinescu, N. D. M. Hine, *Nano Lett.* **2016**, *16*, 2586.

[84] L. Li, G. J. Ye, V. Tran, R. Fei, G. Chen, H. Wang, J. Wang, K. Watanabe, T. Taniguchi, L. Yang, X. H. Chen, Y. Zhang, *Nat. Nanotechnol.* **2015**, *10*, 608.

[85] X. Chen, Y. Wu, Z. Wu, Y. Han, S. Xu, L. Wang, W. Ye, T. Han, Y. He, Y. Cai, N. Wang, *Nat. Commun.* **2015**, *6*, 7315.

[86] Z. Wang, A. Islam, R. Yang, X. Zheng, P. X.-L. Feng, *J. Vac. Sci. Technol. B* **2015**, *33*, 052202.

[87] G. Long, D. Maryenko, J. Shen, S. Xu, J. Hou, Z. Wu, W. K. Wong, T. Han, J. Lin, Y.

Cai, R. Lortz, N. Wang, *Nano Lett.* **2016**, *16*, 7768.

[88] L. Li, F. Yang, G. J. Ye, Z. Zhang, Z. Zhu, W. Lou, X. Zhou, L. Li, K. Watanabe, T. Taniguchi, K. Chang, Y. Wang, X. H. Chen, Y. Zhang, *Nat. Nanotechnol.* **2016**, *11*, 593.

[89] B. Hunt, J. D. Sanchez-Yamagishi, A. F. Young, M. Yankowitz, B. J. LeRoy, K. Watanabe, T. Taniguchi, P. Moon, M. Koshino, P. Jarillo-Herrero, R. C. Ashoori, *Science* **2013**, *340*, 1427.

[90] L. A. Ponomarenko, A. K. Geim, A. A. Zhukov, R. Jalil, S. V. Morozov, K. S. Novoselov, I. V. Grigorieva, E. H. Hill, V. V. Cheianov, V. I. Fal'ko, K. Watanabe, T. Taniguchi, R. V. Gorbachev, *Nat. Phys.* **2011**, *7*, 958.

[91] L. Viti, J. Hu, D. Coquillat, A. Politano, C. Consejo, W. Knap, M. S. Vitiello, *Adv. Mater.* **2016**, *28*, 7390.

[92] C. Chowdhury, S. Karmakar, A. Datta, *ACS Energy Lett.* **2016**, *1*, 253.

[93] Y. Y. Illarionov, M. Waltl, G. Rzepa, J. S. Kim, S. Kim, A. Dodabalapur, D. Akinwande, T. Grasser, *ACS Nano* **2016**, *10*, 9543.

[94] H. Tian, B. Deng, M. L. Chin, X. Yan, H. Jiang, S. J. Han, V. Sun, Q. Xia, M. Dubey, F. Xia, H. Wang, *ACS Nano* **2016**, *10*, 10428.

[95] J. Miao, L. Cai, S. Zhang, J. Nah, J. Yeom, C. Wang, *ACS Appl. Mater. Interfaces* **2017**, *9*, 10019.

[96] M. A. Huber, F. Mooshammer, M. Plankl, L. Viti, F. Sandner, L. Z. Kastner, T. Frank, J. Fabian, M. S. Vitiello, T. L. Cocker, R. Huber, *Nat. Nanotechnol.* **2016**, *12*, 207.

[97] T. Li, P. Sharma, A. Lipatov, H. Lee, J.-W. Lee, M. Y. Zhuravlev, T. R. Paudel, Y. A. Genenko, C.-B. Eom, E. Y. Tsymbal, A. Sinitskii, A. Gruverman, *Nano Lett.* **2017**, *17*, 922.

[98] J.-F. Ge, Z.-L. Liu, C. Liu, C.-L. Gao, D. Qian, Q.-K. Xue, Y. Liu, J.-F. Jia, *Nat. Mater.* **2014**, *14*, 285.

[99] S. Yuan, Z. Yang, C. Xie, F. Yan, J. Dai, S. P. Lau, H. L. W. Chan, J. Hao, *Adv. Mater.* **2016**, *28*, 10048.

[100] W. Jie, Z. Yang, F. Zhang, G. Bai, C. W. Leung, J. Hao, *ACS Nano* **2017**, *11*, 6950.

[101] Z. Yang, W. Huang, J. Hao, *Appl. Phys. Lett.* **2013**, *103*, 31919.

[102] C. Ang, L. E. Cross, Z. Yu, R. Guo, A. S. Bhalla, J. H. Hao, *Appl. Phys. Lett.* **2001**, *78*, 2754.

[103] J. H. Hao, J. Gao, Z. Wang, D. P. Yu, *Appl. Phys. Lett.* **2005**, *87*, 131908.

[104] N. Youngblood, C. Chen, S. J. Koester, M. Li, *Nat. Photonics* **2015**, *9*, 247.

[105] Z. Yang, W. Jie, C.-H. Mak, S. Lin, H. Lin, X. Yang, F. Yan, S. P. Lau, J. Hao, *ACS Nano* **2017**, *11*, 4225.

[106] M. Z. Bellus, Z. Yang, J. Hao, S. Ping Lau, H. Zhao, *2D Mater.* **2017**, *4*, 25063.

[107] J. Hao, W. Si, X. X. Xi, R. Guo, a.S. Bhalla, L. E. Cross, *Appl. Phys. Lett.* **2000**, *76*, 3100.

[108] W. Huang, Z. P. Wu, J. H. Hao, *Appl. Phys. Lett.* **2009**, *94*, 32905.

[109] S. Zhang, N. Mao, J. Wu, L. Tong, J. Zhang, Z. Liu, *Small* **2017**, *13*, 1700466.

[110] V. D. Ganesan, J. Linghu, C. Zhang, Y. P. Feng, L. Shen, *Appl. Phys. Lett.* **2016**, *108*, 122105.

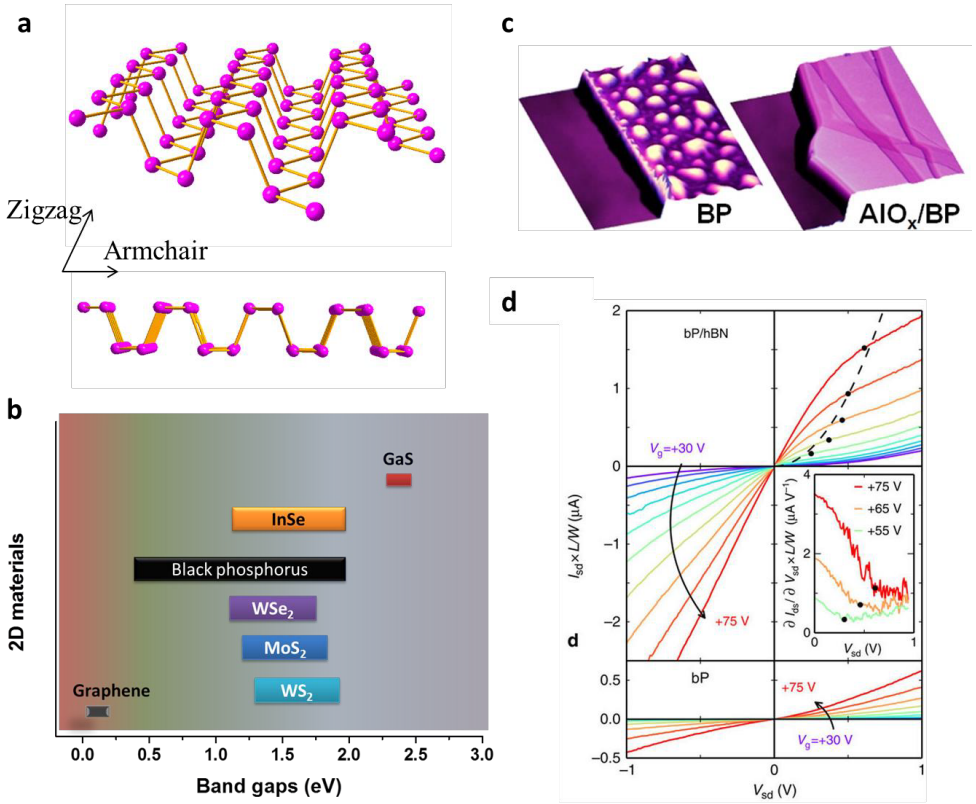

Figure 1. a) The top view and cross-section view of atomic structure of phosphorene. b) Summary of band gap values for common 2D layered materials. c) Comparison of surface morphology between bare BP and AlO_x/BP. Reproduced with permission.[26] Copyright 2014, American Chemical Society. d) Output characteristics for both the passivated and exposed channels of BP FETs. The inset exhibits the conductance at different gate biases. Reproduced with permission.[28] Copyright 2015, Nature Publishing Group.

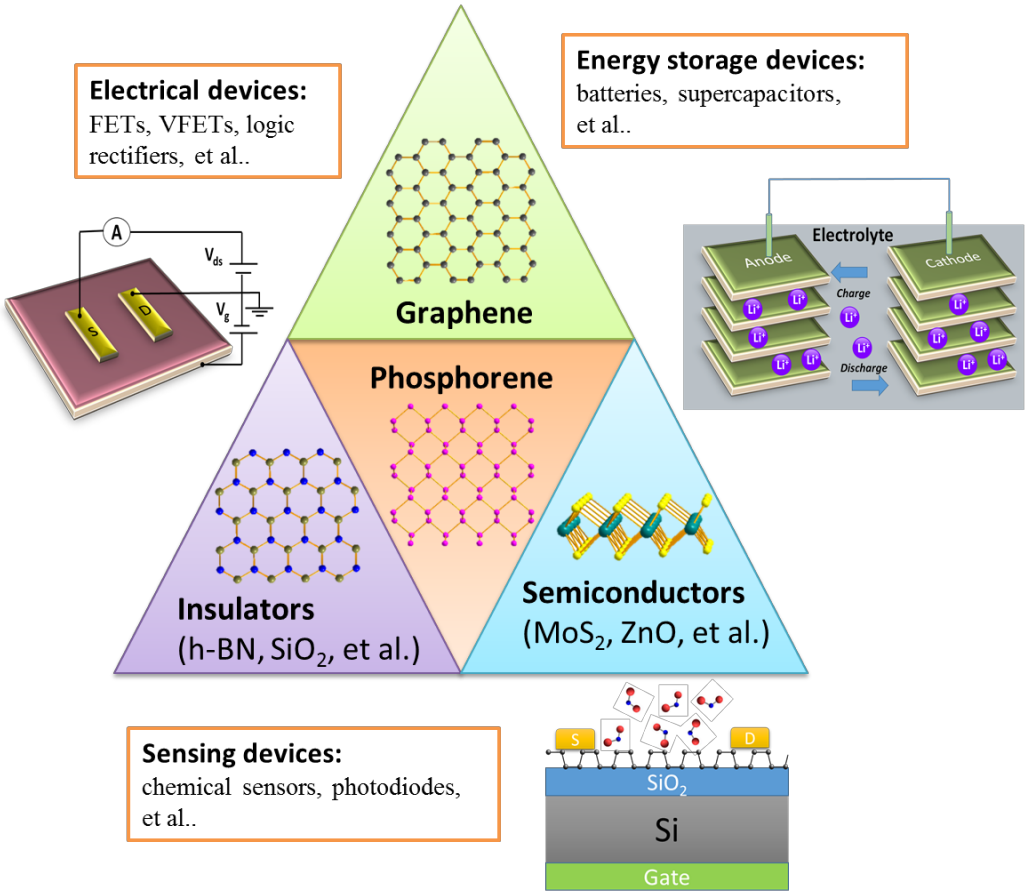

Figure 2. The schematic showing BP based heterostructures and their main device applications.

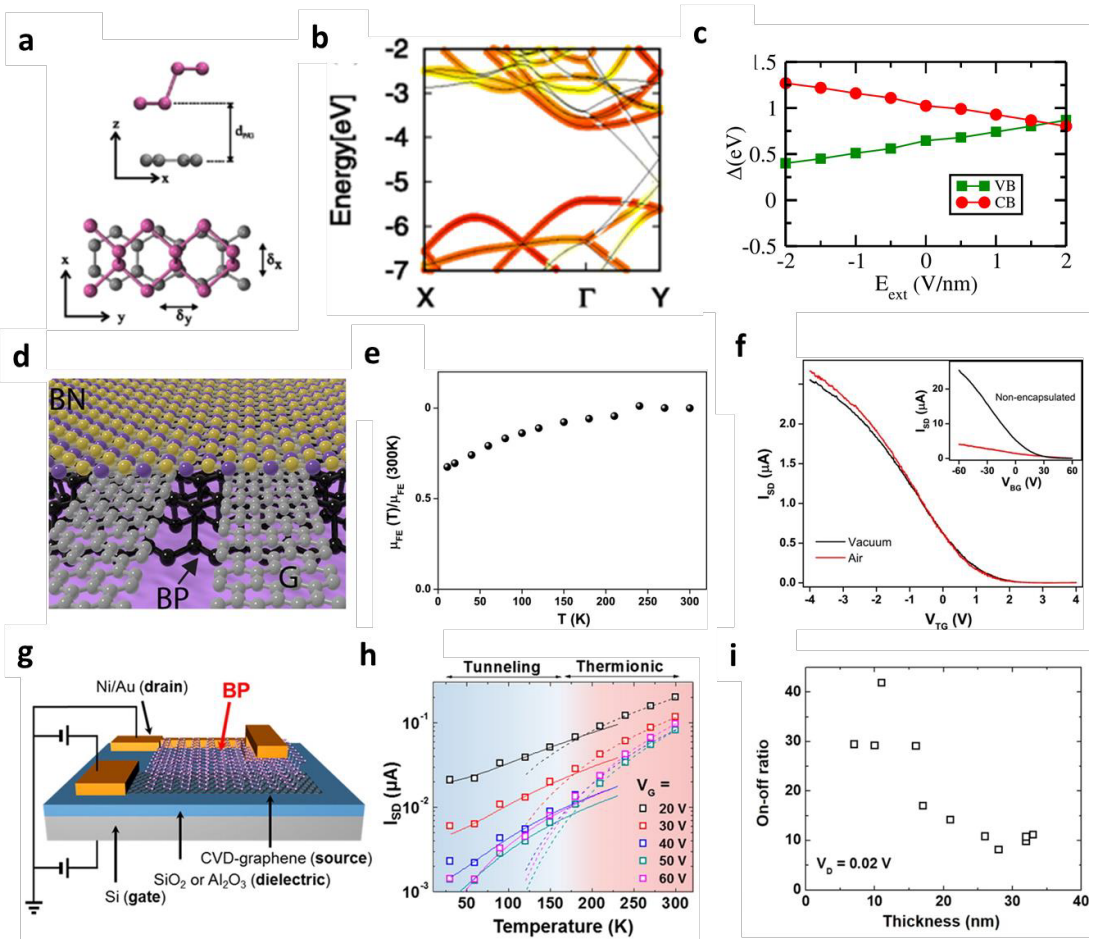

Figure 3. Schematic and performance of electronic devices based on BP-graphene heterostructures. a) Atomic structure of BP-graphene stacks. b) Band structure of phosphorene on top of graphene projected at the phosphorene layer. c) The relationship between evolution of the band edges of phosphorene and the external field relative to the graphene Dirac point. Reproduced with permission.[44] Copyright 2015, American Physical Society. d) Schematic of stacking of BP, h-BN and graphene. e) The field-effect mobility as a function of temperature. f) The drain current as a function of top gate biases for both vacuum and ambient environment. The inset shows the transfer curves of the non-protected device for comparison. Reproduced with permission.[47] Copyright 2015, American Chemical Society. g) Schematic of VFET based on BP-graphene. h) Drain current as a function of temperature under different gate biases. i) Thickness dependent BP-VFET switching ratio at a V_{ds} of 0.02 V. Reproduced with permission.[51] Copyright 2016, American Chemical Society.

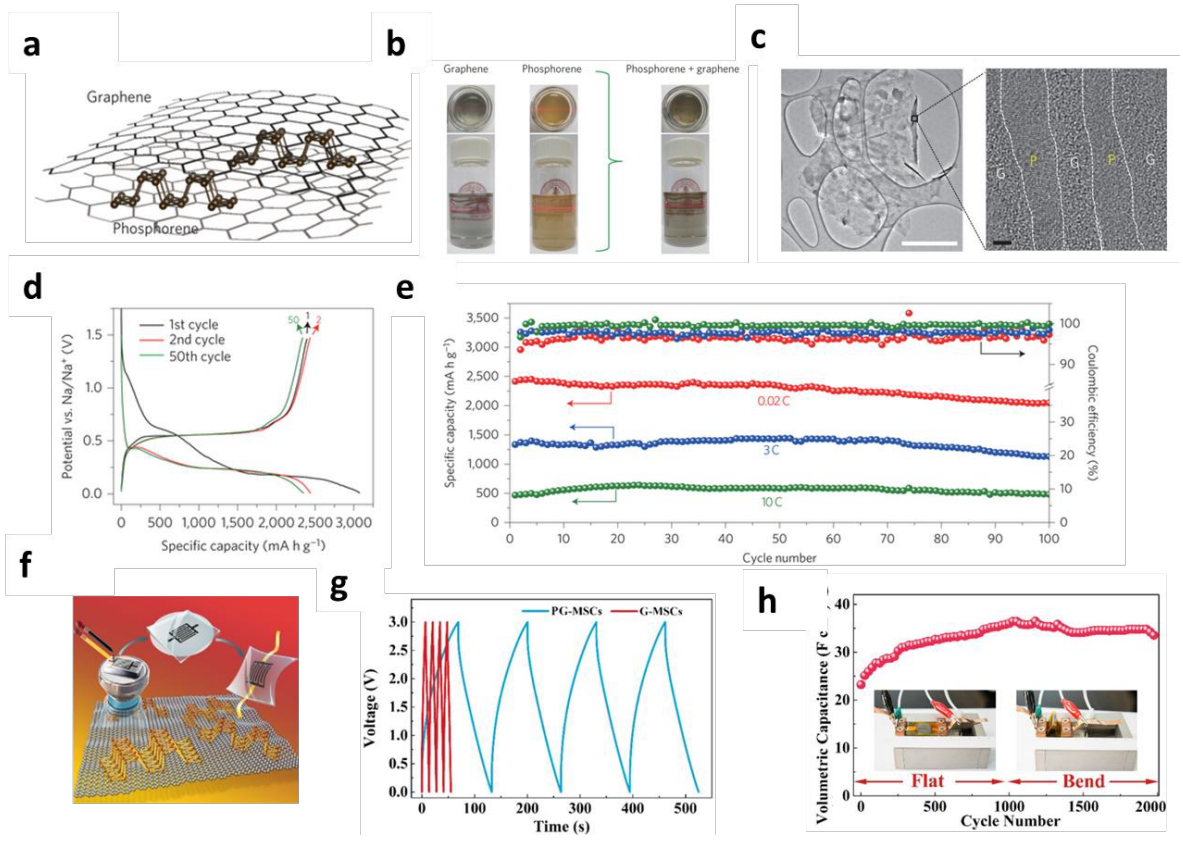

Figure 4. Energy storage devices based on BP-graphene. a) Schematic of the phosphorene-graphene heterostructure. b) Photographs of dispersions of graphene, phosphorene and the heterostructures, respectively. c) TEM image of the phosphorene-graphene system (Scale bar, 2 μm) and cross-sectional TEM image of the sandwiched heterostructure (Scale bar, 2 nm). d) The 1st, 2nd and 50th rounds of discharge-charge curves of sodium-ion batteries with phosphorene-graphene anodes. e) The specific capacity and Columbic efficiency of phosphorene-graphene anodes as a function of cycle number under different currents. Reproduced with permission.[58] Copyright 2015, Nature Publishing Group. f) Schematic of the phosphorene-graphene micro-supercapacitor. g) The galvanostatic charging and discharging characteristics of both PG-MSCs and G-MSCs. h) Volumetric capacitances of PG-MSCs as a function of cycle number, where the device is under flat and bending state each for 1000 cycles. Reproduced with permission.[60] Copyright 2017, American Chemical Society.

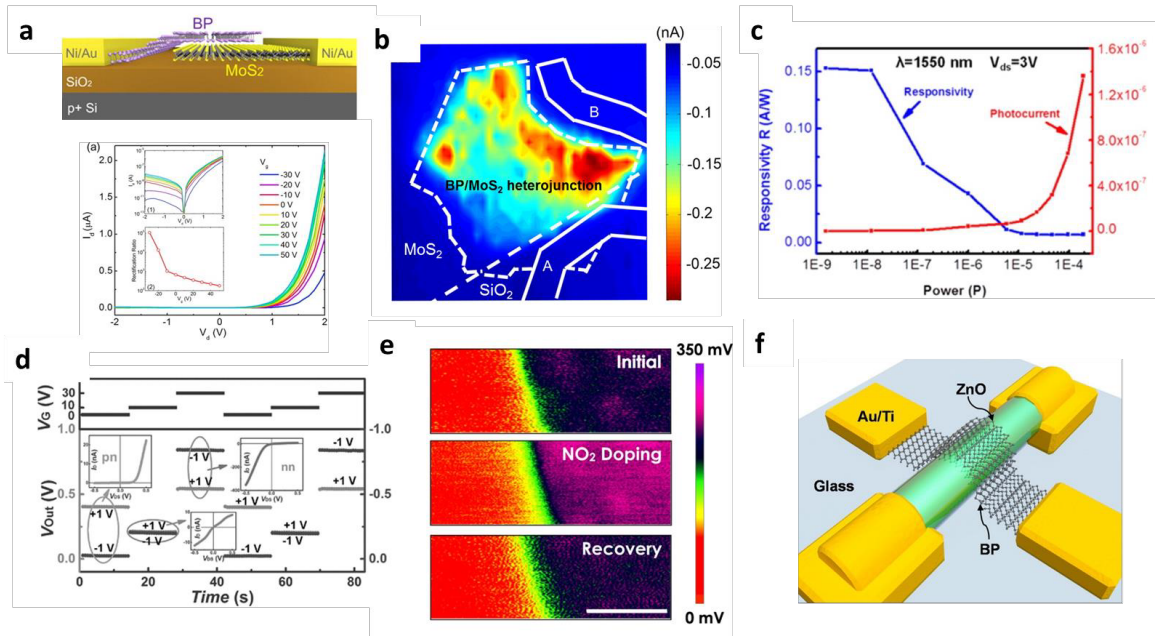

Figure 5. Device applications based on heterostructures of BP-semiconductors. a) The top image shows the cross-section view of BP-MoS_2 based device. The bottom figure shows the transfer curve of the p-n junction. The inset figures exhibit output characteristics and gate voltage dependent rectification ratio of the device, respectively. b) Photocurrent mapping of BP-MoS_2 device. The white dashed lines reveal the region of the p-n junction. Reproduced with permission.[31] Copyright 2014, American Chemical Society. c) The photocurrents and photoresponsivity of the device as a function of incident power intensities. Reproduced with permission.[64] Copyright 2016, American Chemical Society. d) Switching behavior of the circuit by applying different V_g with an input voltage of +1 and -1V. Reproduced with permission.[65] Copyright 2017, Wiley-VCH. e) KPFM results of BP/$MoSe_2$ in the initial state (top), after NO_2 doping (middle) and recovery (bottom). Scale bar is 1μm. Reproduced with permission.[70] Copyright 2016, IOP Publishing Ltd. f) Schematic of device based on BP-ZnO heterojunction. Reproduced with permission.[33] Copyright 2016, American Chemical Society.

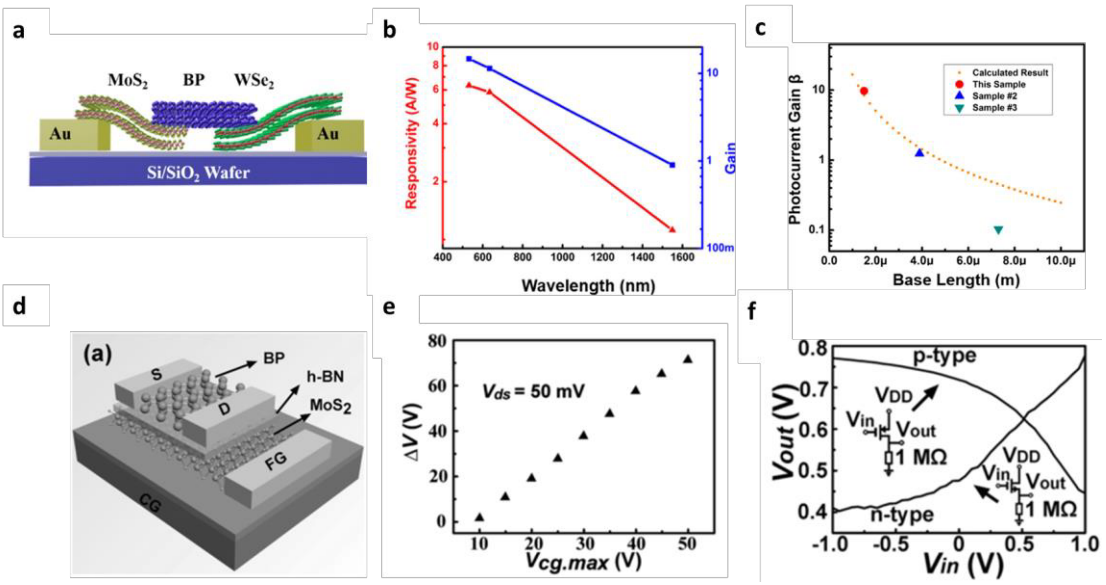

Figure 6. The electronic devices based on multilayered BP heterojunctions. a) Schematic of bipolar junction transistors based on WSe_2/BP/MoS_2. b) Photogain and responsivity of the heterostructure device as a function of illumination wavelength. c) Photocurrent gain of phototransistor based on WSe_2/BP/MoS_2 as a function of length of the base region. Reproduced with permission.[72] Copyright 2017, American Chemical Society. d) Schematic of FGFET based on BP/h-BN/MoS_2. e) The memory window width as a function of $V_{cg.max}$. f) V_{out}-V_{in} curves of both p-type mode and n-type mode of the reconfigurable inverter fabricated by BP/h-BN/MoS_2. The inset shows the schematic circuits of p-type mode and n-type mode, respectively. Reproduced with permission.[75] Copyright 2015, Wiley-VCH.

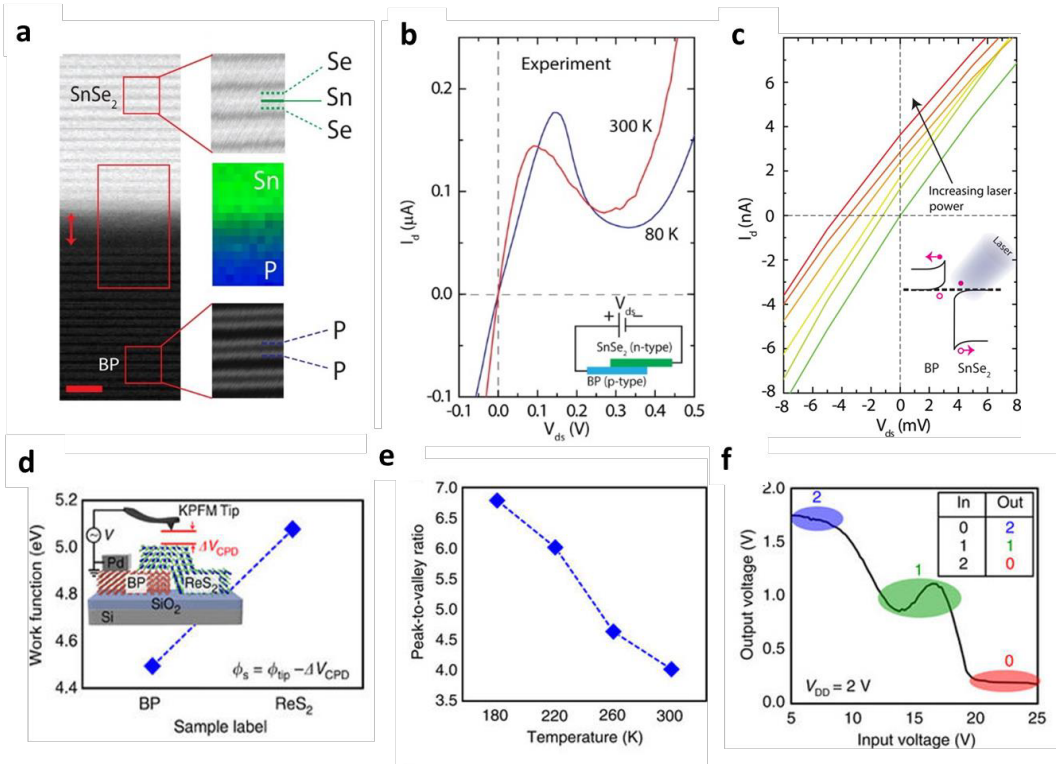

Figure 7. The characterization of negative differential resistance devices based on BP heterostructures. a) Cross-sectional TEM images and EELS mapping of the BP-$SnSe_2$ heterostructure. The scale bar is 2 nm. b) I_d-V_d characteristic measured at temperatures of 300 K and 80 K, respectively. The inset image shows the circuit of the NDR device. c) I_d-V_d characteristics obtained under different laser power. The inset schematic shows the band structure of BP-$SnSe_2$ under illumination. Reproduced with permission.[79] Copyright 2015, American Chemical Society. d) Work functions of both BP and ReS_2. The inset image presents the setup of KPFM for characterizing BP/ReS_2. e) Temperature dependent peak-to-valley ratio of the NDR device based on BP/ReS_2. f) Output voltage of the ternary inverter as a function of input voltage. The inset table summarizes the relationship between input and output signals. Reproduced with permission.[80] Copyright 2016, Nature Publishing Group.

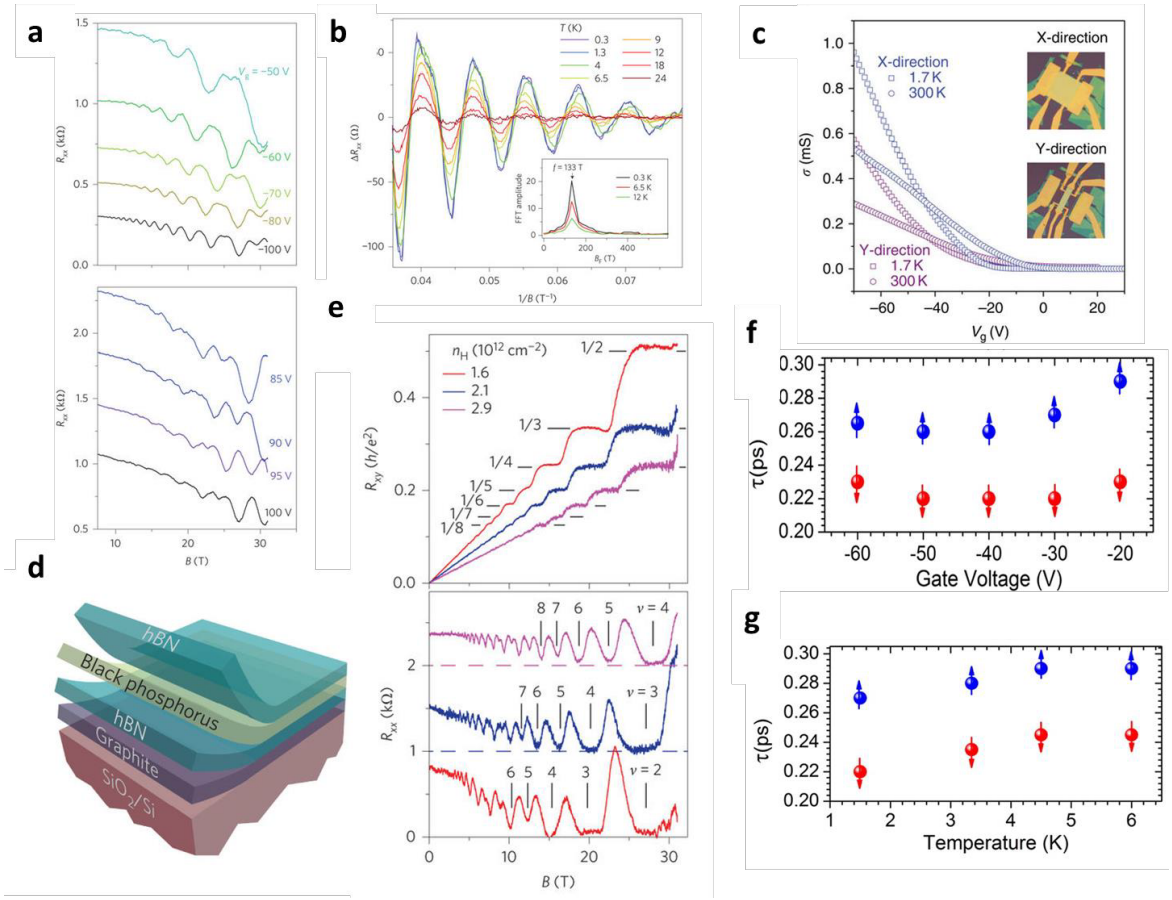

Figure 8. Quantum oscillations in BP/h-BN heterostructures. a) The longitudinal resistance plotted as a function of magnetic field under both different negative and positive gate biases, respectively. b) The longitudinal resistance as a function of 1/B characterized under different temperatures. The gate voltage is fixed at -80 V. The inset shows the Fourier transform of the curve. Reproduced with permission.[84] Copyright 2015, Nature Publishing Group. c) The conductivity of both x- and y- directions of BN-BP-BN heterostructure as a function of gate biases, measured at both 1.7 K and 300 K, respectively. The inset optical images exhibit the setups of the devices measured at different directions. Reproduced with permission.[85] Copyright 2015, Nature Publishing Group. d) Schematic of stacking of h-BN/BP/h-BN on graphite/SiO_2/Si substrate. e) R_{xy} and R_{xx} as a function of the magnetic field measured at different levels of hole doping. The QH effect is clearly observed with more than three well-quantized plateaus. Reproduced with permission.[88] Copyright 2016, Nature Publishing Group. f) The scattering times for both spin-down and spin-up carriers as a function of gate voltages. g) The scattering times for both spin-down and spin-up carriers as a function of temperatures. Reproduced with permission.[87] Copyright 2016, American Chemical Society.

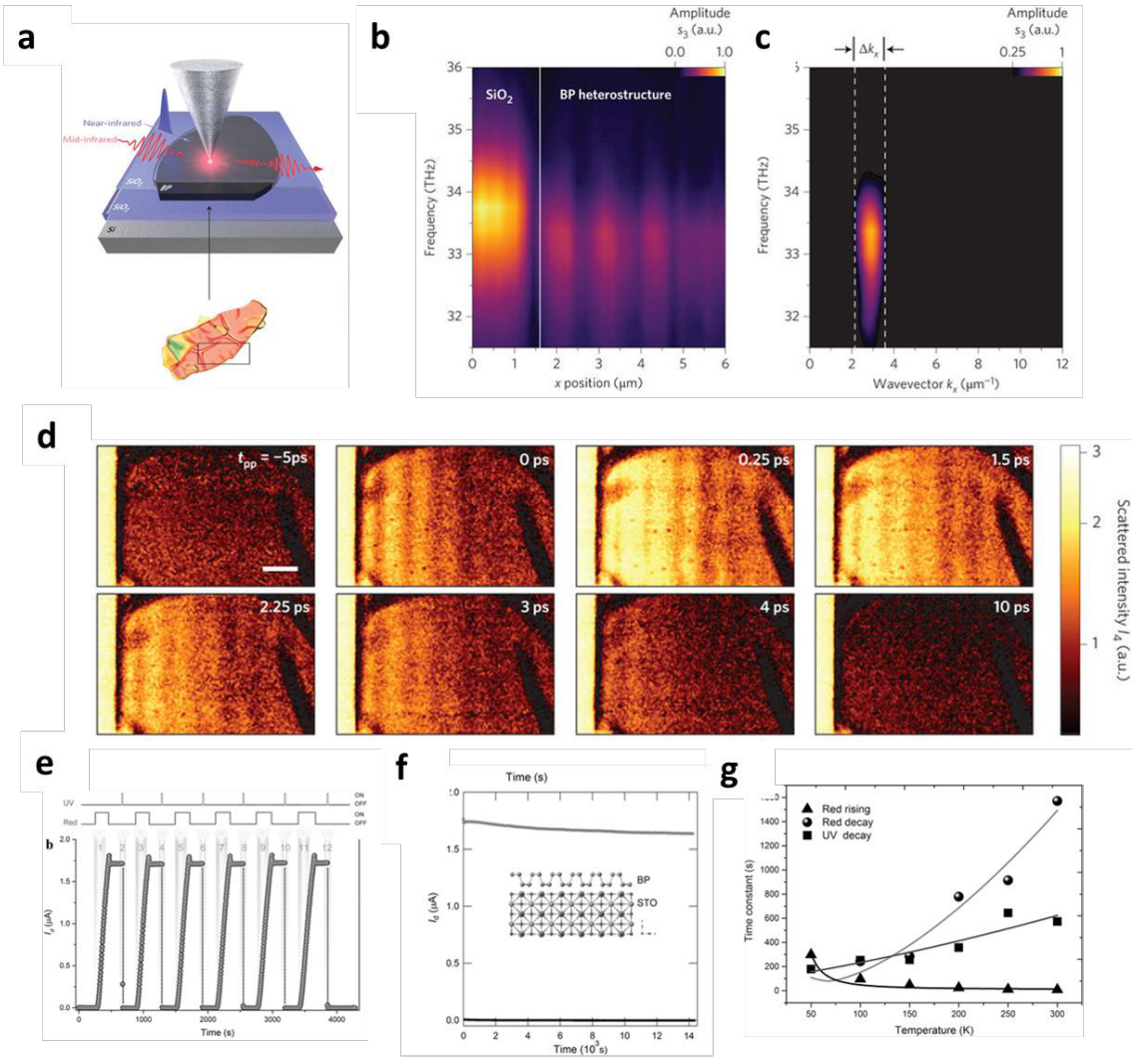

Figure 9. Switchable optical devices based on BP-oxides heterostructures. a) Schematic of the measurement setup with the near-field microscopy system. The bottom shows the optical image of the heterostructure based on phosphorene and SiO_2. b) Hyperspectral mapping of the hybrid mode in SiO_2/BP/SiO_2 heterostructure. c) The Fourier transformation of the hyperspectral map in b). d) Scattered near-field intensity snapshot images of SiO_2/BP/SiO_2 as a function of delay time between pump and probe pulses. The scale bar is 1 μm. Reproduced with permission.[96] Copyright 2016, Nature Publishing Group. e) The photocurrent as a function of illumination time, where both UV and red lights are switched on and off alternatively. f) The photocurrents as a function of decay time at both on and off states, respectively. Inset image shows the schematic of BP/STO based heterostructure. g) Time constants for processes under different illumination as a function of temperature. Reproduced with permission.[34] Copyright 2016, Wiley-VCH.

Table 1. Summary of BP heterostructures and applications

Heterojunction type	Layer structure	Application	Device performance	Ref
Semiconductor-Semi-metal	BP/Graphene	FETs	μ_{FE} = 63 cm^2/V.s on/off ratio = 10^2	[47]
	BP/Graphene	V-FETs	On current density = 1600 A/cm^2 on/off ratio = 800	[51]
	BP/Graphene	Sodium batteries	Specific capacity = 2440 mAh/g	[58]
	BP/Graphene	Micro-supercapacitors	Volumetric capacitance = 37.0 F/cm^3 Energy density = 11.6 mWh/cm^3	[60]
p-n junction	BP/MoS_2	Phototransistors	Responsivity = 418 mA/W	[31]
	BP/MoS_2	NIR-phototransistors	Responsivity = 153.4 mA/W	[64]
	BP/WSe_2	Logic rectifiers	EQE = 23 %	[65]
	BP/$MoSe_2$	Chemical sensors	Response to 25 ppb NO_2 = 10.5 %	[70]
	BP/ZnO	J-FETs	On/off ratio = 10^4	[33]
	BP/$SnSe_2$	Esaki diodes	PVCR = 1.8 at 300 K	[79]
	BP/ReS_2	NDR device	PVCR = 4.2 at 300 K	[80]
n-p-n junction	WSe_2/BP/MoS_2	Bipolar junction transistors	Photoresponsivity (532 nm) = 6.32 A/W Photoresponsivity (1550 nm) = 1.12 A/W	[72]
p-i-n junction	BP/h-BN/MoS_2	Floating-gate FETs	μ_{FE} = 430 cm^2/V.s Memory on/off ratio = 100	[75]
Semiconductor-insulator	BP/h-BN	FETs	μ_{FE} = 45000 cm^2/V.s at 2 K	[87]
	h-BN/BP/h-BN	THz nanodetectors	Responsivity = 1.7 V/W at 295 GHz Responsivity = 0.2 V/W at 593 GHz	[91]
	BP/STO	Photoconductive switch	Responsivity = 10^5 A/W	[34]